Journal of Atmospheric and Solar–Terrestrial Physics 189 (2019) 98–106

Contents lists available at ScienceDirect

Journal of Atmospheric and Solar-Terrestrial Physics

journal homepage: www.elsevier.com/locate/jastp

On the link between atmospheric cloud parameters and cosmic rays

J. Christodoulakis[a,c,*], C.A. Varotsos[a], H. Mavromichalaki[b], M.N. Efstathiou[a], M. Gerontidou[b]

[a] Climate Research Group, Section of Environmental Physics and Meteorology, Department of Physics, National and Kapodistrian University of Athens, Athens, Greece
[b] Cosmic Ray Group, Section of Nuclear and Particle Physics, Department of Physics, National and Kapodistrian University of Athens, Greece
[c] Laboratory of Luminescence Dating, Institute of Nanoscience and Nanotechnology, National Centre for Scientific Research "Demokritos", Agia Paraskevi, Greece

ARTICLE INFO

Keywords:
Cosmic rays
Multifractal detrended fluctuation analysis
Cloud optical thickness
Cirrus reflectance

ABSTRACT

We investigate the cosmic rays behavior with respect to the scaling features of their temporal evolution. Our analysis is based on cosmic rays measurements by three neutron monitor stations in Athens (Greece), Jungfraujoch (Switzerland) and Oulu (Finland), for the period 2000 to early 2017. Each of these datasets was analyzed by using the Detrended Fluctuation Analysis (DFA) and Multifractal Detrended Fluctuation Analysis (MF-DFA) in order to investigate intrinsic properties, like self-similarity and the spectrum of singularities. The main result obtained is that the cosmic rays time series as recorded by the aforementioned neutron monitor stations exhibit positive long-range correlations of $1/f$ type with multifractal behavior meaning that this behavior is characteristic for cosmic rays at North Hemisphere. In addition, we investigate the possible similar scaling features in the temporal evolution of meteorological parameters that are closely associated with the cosmic rays, such as physical properties of clouds. The main conclusions drawn from the latter investigation are that positive long-range correlations are observed in cloud optical thickness liquid mean and cirrus reflectance mean, while both of them do not present statistically significant correlation with cosmic rays, which is in agreement with earlier studies.

1. Introduction

Cosmic rays (CR) are particles coming from stellar sources inside or, outside the solar system, consisting mainly of high energy protons (~89%), alpha particles (~10%) and other heavier nuclei (~1%). In the case where CR originates outside the solar system they are designated as Galactic Cosmic Rays (GCRs). In this regard, high-energy astrophysical processes, such as the supernova, are believed to produce most of the GCRs traveling in the universe (Jackman et al., 2016).

When CR reach the Earth's atmosphere, then showers of muons, electrons, neutrinos, gammas, positrons, neutrons, protons, $\pi+$, $K+$ (i.e. secondary particles) are produced, penetrating deeper in atmosphere and, depending on their energies, reach the Earth's surface, where they are monitored by ground-based detectors. The inventor of the Neutron Monitor was John A. Simpson, in 1948 (Simpson, 2000). In 1965 J. Simpson, along with his students and co-workers, built the first cosmic ray (energy particle) detectors to visit Mars. Simpson was one of the 12 scientists, who organized the program of the 1957–1958 International Geophysical Year (IGY) in order to study cosmic rays, solar physics, and magnetospheric physics, when many stations of the present-day worldwide network, started the continuous registration and monitoring of the cosmic ray variations.

It is worth noting that neutron monitor stations, like the ones used in this study, are recorded the hadronic component of the secondary CRs. These measurements of secondary radiation offer an important tool for the study of primary CRs as they are directly correlated with each other (Simpson, 2000; Paschalis et al., 2014).

Several studies presented their analytical results about the temporal evolution and scaling properties of CR (Kudela and Venkatesan, 1995, 1993; Kudela et al., 1996). For example, Xanthakis et al. (1989), Mavromichalaki et al. (2003), Kudela et al. (2001) reported the temporal evolution of CR daily values based on neutron monitors data at different cutoff rigidities, by applying a wavelet transform tool (time scale ~60–~1000 days).

However, these studies did not lead to a persistent periodicity with the same amplitude for the entire period analyzed. In this regard, McCracken et al. (2004) investigated the long-term modulation of the GCRs over the past 1150 years, using the ^{10}Be data recorded at Greenland and the South Pole and introducing the use of 22-year average intensity of GCR. Greenland data, due to their high temporal

* Corresponding author. Climate Research Group, Section of Environmental Physics and Meteorology, Department of Physics, National and Kapodistrian University of Athens, Athens, Greece.
E-mail address: physjohn@yahoo.gr (J. Christodoulakis).

https://doi.org/10.1016/j.jastp.2019.04.012
Received 16 February 2019; Received in revised form 11 April 2019; Accepted 20 April 2019
Available online 24 April 2019

resolution, indicated that there were significant 11-year, and also other, fluctuations superimposed upon the high GCR intensities during the Spörer and Maunder solar activity minima (i.e. 1460 to 1550 and 1645 to 1715, respectively). These findings have demonstrated the continued presence of an effective and time-dependent heliomagnetic field. McCracken et al. (2004) also stressed that the modulation (i.e., depression) of the cosmic ray intensity during the instrumental era (1933–present) was one of the largest in the past 1150 years. They, by interpreting their results, concluded also that the long-term variations in the GCR intensity are poorly related to sunspot number during periods of low solar activity. Finally, McCracken et al. (2004) showed that there is a relatively good correlation between variations in the ^{10}Be data and changes in the solar magnetic flux predicted by Solanki et al. (2002) and Schrijver and Derosa (2002) models, but there are significant differences among these models and ^{10}Be data over specific periods.

In addition, potential mechanisms assuming geomagnetic field - GCR influence on the ozone content need further exploration given that both air-pollution and ozone layer depletion problems are of great importance for the environment (Varotsos and Cartalis, 1991; Varotsos, 2002; Cracknell and Varotsos, 2007; Cracknell et al., 2009; Varotsos et al., 2009a, b; Tidblad et al., 2012; Krapivin et al., 2015; Chattopadhyay et al., 2019). In this context, possible geomagnetic field - CR influence on the ozone content is possible through the dependence of the CR induced ionization on the changes of the geomagnetic field. The CR induced ionization depends on geomagnetic cutoff rigidity. Then migration of the geomagnetic poles may alter the CR induced ionization in some regions on time scales of centuries. However, the problem is that the ozone production by CR is too small (e.g. Jackman et al., 2016). Another way for the geomagnetic field impact on the ozone is through particle precipitations which produce odd nitrogen (NOx) in the high-latitude mesosphere/lower thermosphere region. During polar winter, and particularly during SSW events, the NOx is long-lived and can be transported down to the stratosphere where it destroys stratospheric ozone. Since particle precipitation is affected by the geomagnetic field then changes in the positioning of the magnetic poles, i.e. their migration, could modify this downward coupling mechanism (e.g. Baumgaertner et al., 2011).

Moreover, it is widely referred that cosmic rays seed clouds by ionizing molecules in Earth's atmosphere that draw in other molecules to create the aerosols around which water vapour can condense to form cloud droplets. A proposed mechanism of GCRs - cloud - climate that has received the most attention is the ion-aerosol clear-sky hypothesis [Carslaw et al., 2002]. According this hypothesis an increase in GCR to the atmosphere (which happens during the different phases of the solar cycle) leads to an increase in small ions (charged molecules or charged small clusters of molecules) in the troposphere. An increase in small ions may increase the nucleation rate (the formation rate) of ~1 nm diameter aerosol particles. If these new 1 nm particles grow to diameters larger than ~50–100 nm through condensation of vapors (generally sulfuric acid and low-volatility organics), these particles may act as cloud condensation nuclei (CCN). However, the growth to CCN sizes must occur before the new particles are lost by coagulation with existing CCN particles (Pierce and Adams, 2007). An increase in CCN would lead to an increase in cloud droplet number, which may lead to an increase in cloud albedo and cloud cover.

In a recent work Svenmark et al. (2016) analyzed four independent atmospheric data sets a) AERONET data related to the fine aerosol fraction, b) measures for the cloud liquid water content over the ocean, c) data for total cloud fraction and d) data allowed the study of the cloud microphysical parameters together with neutron monitor data. They found high responses greater than 95% to cosmic ray decreases -called Forbush Decreases-in almost all above parameters. A positive non-zero relation between the strength of Forbush decrease and the size of the responses found in all data sets is also determined.

The present study aims to investigate the temporal evolution of cosmic rays, along with the intrinsic self-similarity and spectrum of singularities in their time series, using the daily CR intensity values of the neutron monitoring stations obtained through the Neutron Monitor DataBase (NMDB) and to explore plausible connections with cloud parameters.

2. Data and analysis

The High-Resolution Neutron Monitor DataBase-NMDB (http://www.nmdb.eu/) was founded 10 years ago under the European Union's FP7 program providing 1-min cosmic ray data from the real-time neutron monitoring stations. It is known for its successful and continuous operation, officially distributing data of the neutron monitoring stations for several applications (Mavromichalaki, 2010). For the purposes of the present study the datasets of four of these stations, located at Athens (Greece), at Jungfraujoch (Switzerland) and at Oulu (Finland), were used (all data available at http://www.nmdb.eu/nest/).

The Athens NM64 NM Neutron Monitoring Station (A.Ne.Mo.S) (37.97° N, 23.78° E, altitude: 260m asl, effective vertical cutoff rigidity: 8.53 GV) initiated its activity in November 2000 (Mavromichalaki et al., 2001) is continuously operated till now and is supported by The faculty of Physics of the National and Kapodistrian University of Athens. From the website of this station (http://cosray.phys.uoa.gr) 1-min and 1-h data are available online in digital and graphic form, while the resolution of the measurements reaches up to 1-sec. The Athens Neutron MOnitoring DAta Processing (ANMODAP) Center has been established and is operating since 2003 at the A.Ne.Mo.S. ((Mavromichalaki et al., 2009). Currently on behalf of all real time neutron monitoring stations of the NMDB Database, A.Ne.Mo.S provides in real time two services to the ESA SSA R-ESC, GLE Alert and Multi-station, monitoring and forecasting of the ground level enhancements of cosmic ray intensity (Souvatzoglou et al., 2014; Mavromichalaki et al., 2018; http://swe.ssa.esa.int/space-radiation).

The Jungfraujoch IGY NM station (JIGYNM) (46.55° N, 7.98° E, altitude: 3570m asl, effective vertical cutoff rigidity: 4.5 GV) and Jungfraujoch NM64 NM station (JNM64NM) (46.55° N, 7.98° E, altitude: 3475m asl, effective vertical cutoff rigidity: 4.5 GV) initiated their activities in October 1958 and January 1986, respectively. They are two of the oldest NM stations with continuous operation worldwide. The operation of both stations is supported by the Physikalisches Institut of the University of Bern and by the International Foundation High Altitude Research Stations Jungfraujoch and Gornergrat (HFSJG) in Bern.

The Oulu NM64 NM station (OULU) (65.05° N, 25.47° E, altitude: 15m asl, Geomagnetic cutoff: 0.8 GV) initiated its activity in April 1964. It is operated by Sodankyla Geophysical Observatory of the University of Oulu, Finland.

The daily cosmic ray intensity data obtained at the Athens, Jungfraujoch and Oulu stations are used in the present analysis, after their corrections for pressure and efficiency over the periods 10/11/2000–31/03/2017 for A.Ne.Mo.S and 01/01/2000–31/03/2017 for JIGYNM, JNM64NM and OULU.

To investigate the intrinsic dynamics of the data collected at the above-mentioned measuring sites, the detrended fluctuation analysis (DFA) was used, which eliminates the noise of non-stationary time series and detects their scaling features (Efstathiou and Varotsos, 2010; Peng et al., 1994; Varotsos, 2005; Varotsos et al., 2007, 2005; 2006, 2013a; b; 2003; Weber and Talkner, 2001; Sarlis et al. 2013).

The main idea behind DFA technique is the removal of seasonal variations and non-stationarities from a time series by dividing it into different windows of equal length, τ, and studying among windows the characteristics of the plausible scaling dynamics. It provides a relationship between the root mean square fluctuations $F_d(\tau)$ and the window size τ. investigating their connection via a power-law $F_d(\tau) \propto \tau^{\alpha}$. Note that $F_d^2(\tau)$ stands for the average of the summed squares of the residual found in the windows. The 2nd order polynomial regressor in the DFA is typically denoted as DFA2 (with unlabeled DFA often referring to DFA1). The exponent α is the scaling exponent, which is basically a self-affinity parameter indicating the long-range power-law correlation properties of the analyzed time-series (fractal properties). The value $\alpha = 0.5$ represents white noise, $\alpha < 0.5$ indicates antipersistent long range correlations, and $\alpha > 0.5$ characterizes persistent long range correlations. A detailed description of the DFA sequential steps is given in Eftstathiou et al. (2011), as well as in Varotsos et al. (2009a).

Additionally, we examined whether cosmic ray fluctuations have multifractal nature. For this purpose we used the MultiFractal Detrended Fluctuation Analysis (MF-DFA) to examine the singularity spectrum of the cosmic rays time series and to estimate the multifractality degree. The generalized MF-DFA procedure was proposed by Kantelhardt et al. (2002), where its sequential steps are described in detail.

In our analysis the annual cycle that characterizes the cosmic rays time series was removed by using the average values of CR_{mean} for each calendar day, which were calculated over the entire period 2000–2017 and subtracted from the corresponding CR time series of the relevant day. The long-term trend of CR time series was removed using the polynomial (of 6th degree) regression analysis. The CR time series that is finally obtained is noted as CR_{net}.

In addition, the existence of the long-range correlations in the CR_{net} time series was established by studying the autocorrelation function and the local slopes of the fluctuation function (proposed by Maraun et al., 2004).

Finally, we attempted a comparison between CR_{net} time series and the time series of two meteorological parameters describing physical properties of clouds, such as cloud optical thickness liquid mean and cirrus reflectance mean. Daily data of both parameters obtained from the NASA Giovanni website (http://disc.sci.gsfc.nasa.gov/giovanni) were used covering the period July 2002 to March 2017. These measurements were retrieved from the Moderate Resolution Imaging Spectroradiometer (MODIS) on the Terra research satellite (1° lat × 1° long gridded).

3. Discussion and results

For the purposes of the present study the first step of our work was to investigate the possible existence of self-similarity in the CR time series, for the periods 10/11/2000–31/03/2017 at A.Ne.Mo.S and 01/01/2000–31/03/2017 at IGYNM, JNM64NM and OULU. The results obtained from the analysis performed in the time series of the cosmic ray data are presented for each station just below. The analysis was performed in the common data period so that the results obtained to be comparable.

3.1. The case of the Athens NM64 neutron monitor station

The CR_{net} time series at A.Ne.Mo.S is shown in Fig. 1a, and the corresponding root-mean-square fluctuation function $F_d(\tau)$ versus time scale τ (in days), is depicted in Fig. 1b.

The scaling exponent extracted from the DFA2 application on the above described time series was found $\alpha = 1.08 \pm 0.01$, suggesting long-range persistence (of 1/f – type). However, the establishment of the power-law long-range correlations in the CR_{net} time series requires the necessary investigation of the rejection of the exponential decay of the autocorrelation function and the constancy of “local slopes” in a certain range towards the low frequencies (Maraun et al., 2004).

In more detail, since the single straight line of the DFA2 plot for the CR_{net} time series (at A.Ne.MO.S) detected in the entire range of scales (with slope $\alpha = 1.08$) might be biased, we evaluated the local slopes of $\log F_d(\tau)$ vs. $\log\tau$ (separately for two different window sizes of 15 and 20 points, which were shifted successively over all the calculated scales τ), asking for constancy in a sufficient range. To this aim, we performed Monte Carlo simulations applying the DFA2 method on 500 time series characterized by fractional Gaussian noise (with $\alpha = 1.08$) in order to calculate the local slopes-$\alpha(\tau)$ for each of the 500 time series, at a window of 15 points that was shifted successively over all the calculated scales τ (Timmer and König, 1995).

It is worthy of note that the Kolmogorov–Smirnov (Stephens, 1974) and Anderson–Darling (Anderson and Darling, 1954) best fit tests showed that, for a fixed scale τ, the dataset of the derived local slopes-$\alpha(\tau)$ obey Gaussian distribution (at 95% confidence level). As estimates of the 95% confidence bands we consider $\alpha(\tau) \pm 2\sigma_{\alpha(\tau)}$.

In the following, we attempted to determine a range R for the α-local slopes of the CR_{net} time series, based on their mean value increased and decreased by the two standard deviation $s_{a(\tau)}$, as derived from the 500 estimated local slopes-$\alpha(\tau)$, i.e. $R = (,\ \alpha + 2\sigma_{\alpha(\tau)})$. Thus, according to Fig. 2a, all the local slopes (after the scale $\log\tau = 1.8$) lie within the borders range R, suggesting a sufficient constancy.

Fig. 2b presents the profile of the power spectral density for the CR_{net} time series at A.Ne.Mo.S, showing that the power-law fit gives higher coefficient of determination compared to that of the exponential fit. Thus, both criteria of Maraun et al. (2004) are satisfied and therefore the long-range correlations of power-law type for the CR time series at the Athens station are established.

Furthermore, to examine whether the aforementioned value of the DFA2-exponent ($\alpha = 1.08$) is attributed to the temporal evolution of CR_{net} values and not from their marginal distribution, the examined time series was randomly shuffled. If the shuffled CR_{net} values followed the random (white) noise, then the persistence found above would not come

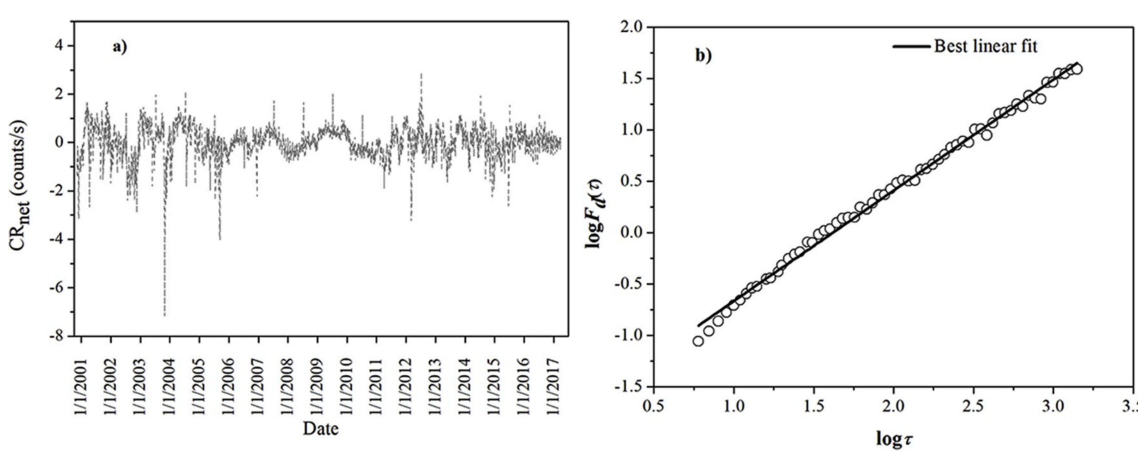

Fig. 1. a) Time series of CR_{net} daily values (after removing long-term trend and annual cycle), during the period 10/11/2000–31/03/2017 at A.Ne.Mo.S. b) The corresponding root-mean-square fluctuation function $F_d(\tau)$ of DFA2 versus time scale τ (in days), in log-log plot and the corresponding best fit equation ($y = 1.08x - 1.74$, with $R^2 = 0.996$) (solid line).

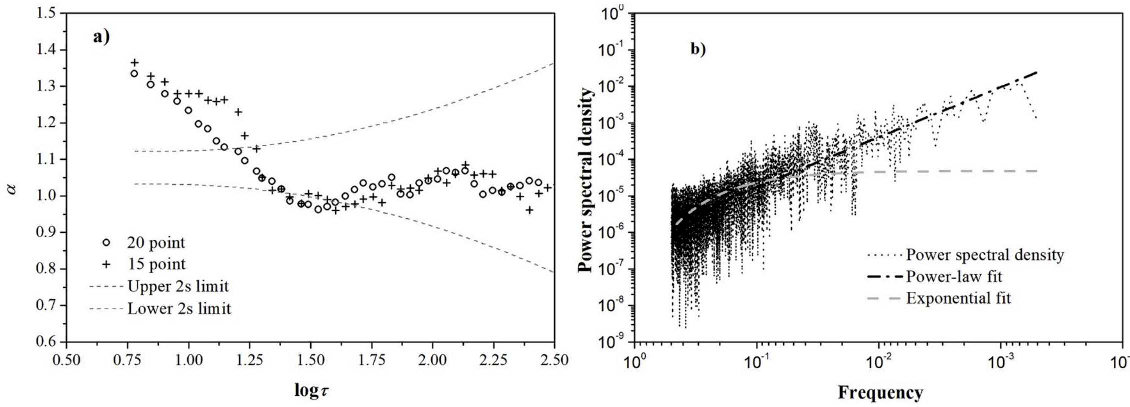

Fig. 2. a) Local slopes of the $\log F_d(\tau)$ vs. $\log\tau$ (10-base logarithms) calculated within a window of 15 points (crosses +) and of 20 points (circles o) for the CR_{net} time series at A.Ne.MO.S. The dashed grey line indicates the corresponding 2σ intervals around the mean value of local slopes (). b) Power spectral density for the above mentioned time series, with the corresponding power-law (black dash dot line) and the exponential (grey dash line) fit ($y = 7.34{\cdot}10^{-7}x^{-1.37}$, with $R^2 = 0.45$ and $y = 4.84{\cdot}10^{-5}e^{-7.39x}$, with $R^2 = 0.32$).

from the data but from their temporal evolution. To this aim, we applied the Monte Carlo method, relying on 1000 repeated random samplings of the CR_{net} dataset of A.Ne.Mo.S to estimate the exponents obtained. According to the Kolmogorov–Smirnov (Stephens, 1974) and Anderson–Darling (Anderson and Darling, 1954) bestfit tests, the dataset of the derived α''-exponents obeyed Gaussian distribution at 95% confidence level with mean value and standard deviation $\sigma_{\alpha''} = 0.08$.

Moreover, the 95% confidence interval of α'' was $\left(\alpha'' - 1.96\frac{\sigma_{\alpha''}}{\sqrt{1000}}, \alpha'' + 1.96\frac{\sigma_{\alpha''}}{\sqrt{1000}}\right)$. Thus, according to the t-test, the estimated DFA exponents depicted of CR_{net} time series (at A.Ne.Mo.S), $\alpha = 1.08$, does not obviously belong to 95% confidence interval of α'' (i.e. white noise) confirming thus the long-range persistent behavior.

Our next step was to study the spectrum of singularities for the CRnet time series, at A.Ne.Mo.S, employing the MF-DFA, which is mainly based on the scaling of the q-th order moments depending on the signal length, and as has been mentioned in the Introduction is a generalization of the standard DFA. In this context, MF-DFA2 technique uses only the second

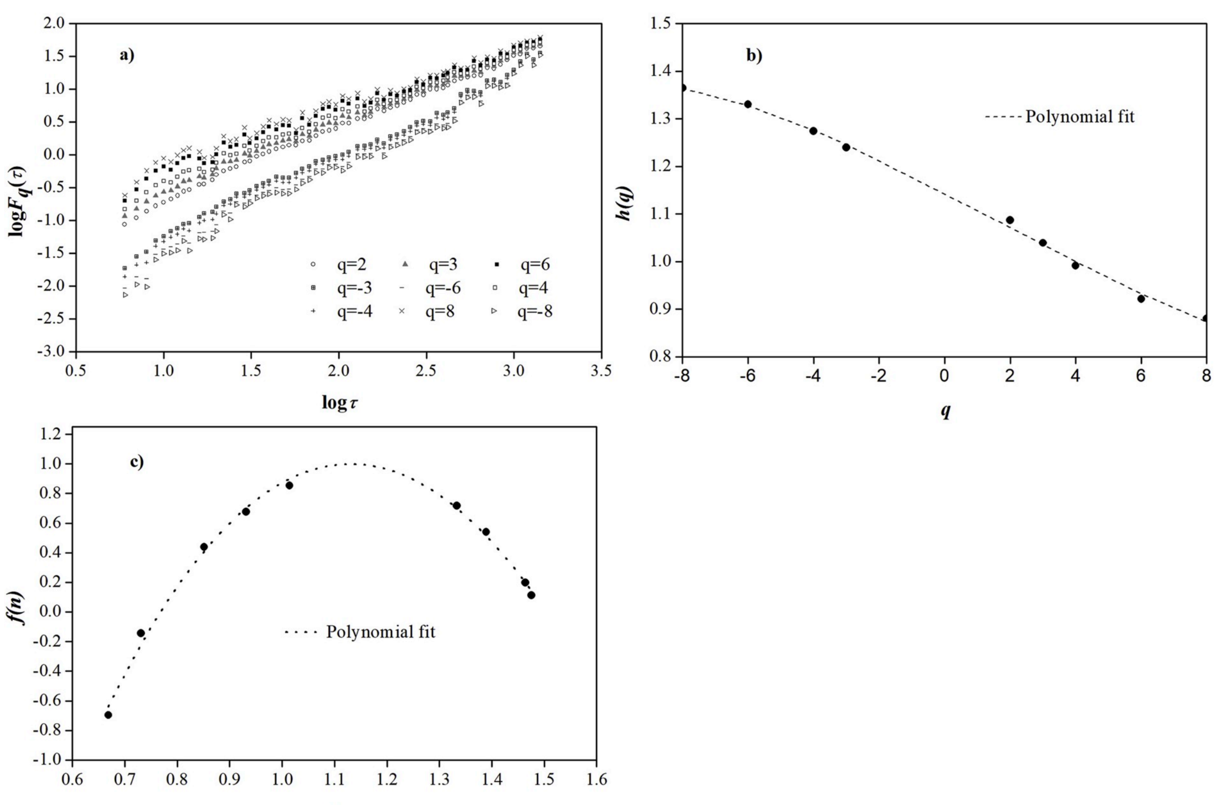

Fig. 3. a) The log-log plots of the MF-DFA2 fluctuation factor $F_q(s)$ versus the time scale s for specific moments q for the CR_{net} time series (at A.Ne.Mo.S). b) The generalized Hurst exponent $h(q)$ versus q for the examined time series. The empirical curve (dots) is fitted by the polynomial of the third order ($y = 8{\cdot}10^{-5}x^3 - 0.0004x^2 - 0.036x + 1.14$, with $R^2 = 0.998$) (dashed line, upper right panel). c) The singularity spectrum $f(n)$ versus singularity strength n for the examined time series. The empirical curve (dots) is fitted by the polynomial of third order ($y = 0.61x^3 - 9.46x^2 + 19.06x – 9.3$, with $R^2 = 0.993$) (solid line).

moment q = 2 and calculates the qth order fluctuation function $F_q(\tau)$ for various moments q. According to Fig. 3a, the scaling behavior of $F_q(\tau)$ (i.e. slope) for all the selected positive (negative) moments q is almost the same for $\log\tau > 2$ ($\tau > 100$), but not for smaller time scales ($\tau < 100$), where the slope of $F_q(\tau)$ increases for less positive (more negative) moments q. This behavior indicated the existence of a great degree of multifractality only for smaller time scales ($\tau \leq 100$), a fact that is expected as the large windows cross several local periods with both small and large fluctuations (i.e. negative and positive q, respectively) and will therefore average out their differences in magnitude (Ihlen, 2012).

The above suggested multifractality is illustrated in Fig. 3b, where the generalized Hurst exponent $h(q)$ for the CR_{net} time series (at A.Ne.Mo.S) varies versus q values (i.e. $h(q)$ is not independent of q), while the $h(q)$ values which are higher than 0.5 indicate long-term persistence for the examined time series.

Moreover, the slope of $h(q)$ for positive moments seems to be similar to that of negative moments, a fact which is in agreement with the findings of Fig. 3a.

Finally, Fig. 3c presents the singularity spectrum $f(n)$ as a function of the singularity strength n for the examined CR_{net} time series (see Kantelhardt et al., 2002). The maximum value of $f(n)$ corresponds to $q = 0$, while $f(n)$ values on the left (right) of the maximum value correspond to positive (negative) moments q. It is apparent that $f(n)$ fluctuates similarly on both sides of its maximum value. This fact reveals once more common features of multifractality for positive and negative q-values.

3.2. The case of the Jungfraujoch NM64 NM station

We apply the above described analysis to the CR_{net} time series at Jung NM64NMs (see Fig. 4a). The corresponding root-mean-square fluctuation function $F_d(\tau)$ of the DFA2 technique versus time scale τ (in days), is shown in Fig. 4b.

The scaling exponent stemmed from the DFA2 tool for the above described time series is almost equal to that one of the CR_{net} time series at Athens station, suggesting once more persistent memory (of 1/f – type) behavior. However, to establish the power-law long-range correlations for the CR_{net} time series (at JNM64NM) we investigated whether the two criteria proposed by Maraun et al. (2004) are satisfied. More specifically, we evaluated the local slopes of $\log F_d(\tau)$ vs. $\log\tau$, which belong within the range R over all the calculated scales τ, indicating once more constancy (Fig. 5a).

On the other hand, power-law fit on the profile of the power spectral density for the CR_{net} time series at JNM64NM, seemed to give a better coefficient of determination compared to that of the exponential fit (Fig. 5b). Thus, both criteria of Maraun et al. (2004) suggest again long-range correlations of power-law type for the CR_{net} time series at Jungfraujoch station.

Regarding the spectrum of singularities for the CR_{net} time series, at JNM64NM, we employed again the MF-DFA2 which gave similar results with those ones of the Athens station (see Fig. 6).

3.3. The case of the Jungfraujoch IGY NM station

For comparison reasons we examined the case of JIGYNM by applying the above mentioned analysis to the CR_{net} time series. The corresponding root-mean-square fluctuation function $F_d(\tau)$ of the DFA2 technique versus time scale τ (in days) gave scaling exponent ($\alpha = 1.09 \pm 0.01$) indicating again persistent memory (of 1/f – type). Moreover, the two criteria proposed by Maraun et al. (2004) revealed constancy of local slopes and power-law long-range correlations for the CR_{net} time series (at JIGYNM) (see Table 1).

As far as the spectrum of singularities for the CR_{net} time series, at JIGYNM, we used again the MF-DFA2 which confirmed the results which were found at A.Ne.Mo.S and JNM64NMs (see Table 1).

3.4. The case of the Oulu neutron monitor station

Our last step was the case of OULU station. The application of the DFA2 technique to the CR_{net} time series versus time scale τ (in days) gave scaling exponent ($\alpha = 1.11 \pm 0.01$), which denotes once more persistency (of 1/f – type).

At the same time, the two criteria proposed by Maraun et al. (2004) revealed again constancy of local slopes and power-law long-range correlations for the CR_{net} time series (at OULU) (see Table 1).

Finally, the MF-DFA2 used to study the spectrum of singularities for the CR_{net} time series, at OULU, gave almost the same results with those ones of A.Ne.Mo.S, JIGYNM and JNM64NMs (see Table 1).

3.5. Comparison between cosmic rays and cloud physical parameters

The main result obtained from the above described analysis is that the cosmic rays time series at all the neutron monitor stations exhibit positive long-range correlations (of 1/f type) with multifractal behavior.

To this point, we try to investigate the possible existence of similar scaling features in the time series of cloud physical parameters which are, according to some views in literature (Svensmark et al., 2009), closely associated with the cosmic rays, such as cirrus reflectance mean (CRM) and cloud optical thickness liquid mean (COTLM). Daily data of both parameters were used covering the period July 2002 to March 2017, for the greater area over central Aegean Sea (22.5°W, 25.5°E,

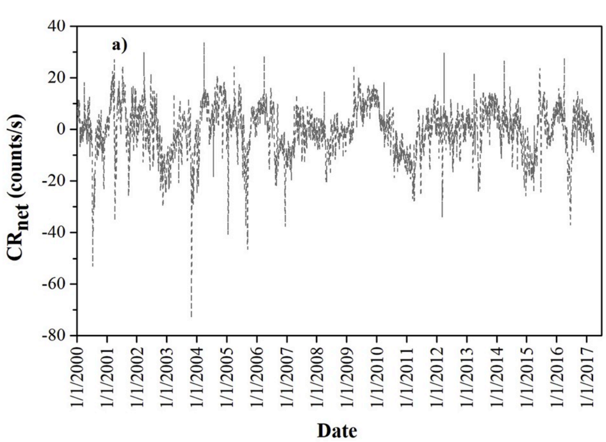

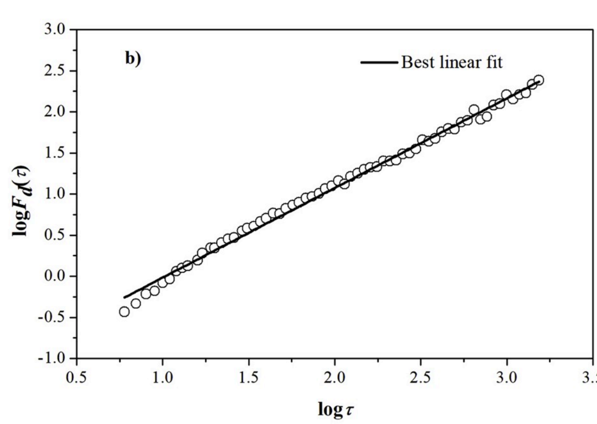

Fig. 4. a) Temporal march of CR_{net} daily values (after removing trend and annual cycle), during the period 01/01/2000–31/03/2017 at JNM64NM. b) The corresponding root-mean-square fluctuation function $F_d(\tau)$ of the DFA2 versus time scale τ (in days), in log-log plot and the corresponding best fit equation ($y = 1.13x - 0.7$, with $R^2 = 0.995$) (solid line).

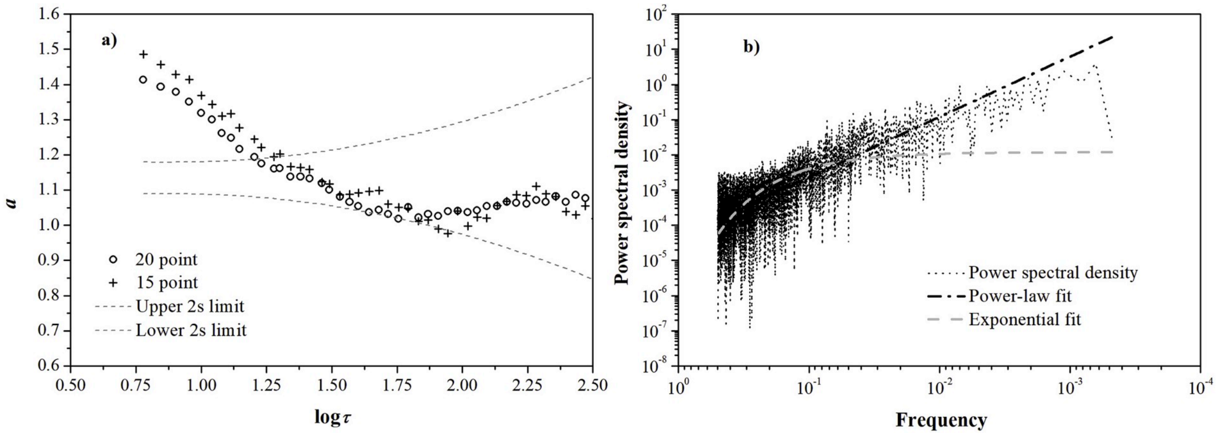

Fig. 5. a) The local slopes of $\log F_d(\tau)$ vs. $\log\tau$ (10-base logarithms) calculated within a window of 15 points (+) and of 20 points (o) for the CR_{net} time series at JNM64NMs. The dashed grey line indicates the corresponding 2σ intervals around the mean value of local slopes ($\alpha = 1.13$). b) The power spectral density for the above mentioned time series, with the corresponding power-law (black dash dot line) and the exponential (grey dash line) fit ($y = 4.4{\cdot}10^{-5}x^{-1.72}$, with $R^2 = 0.6$ and $y = 1.19{\cdot}10^{-2}e^{-10.8x}$, with $R^2 = 0.51$).

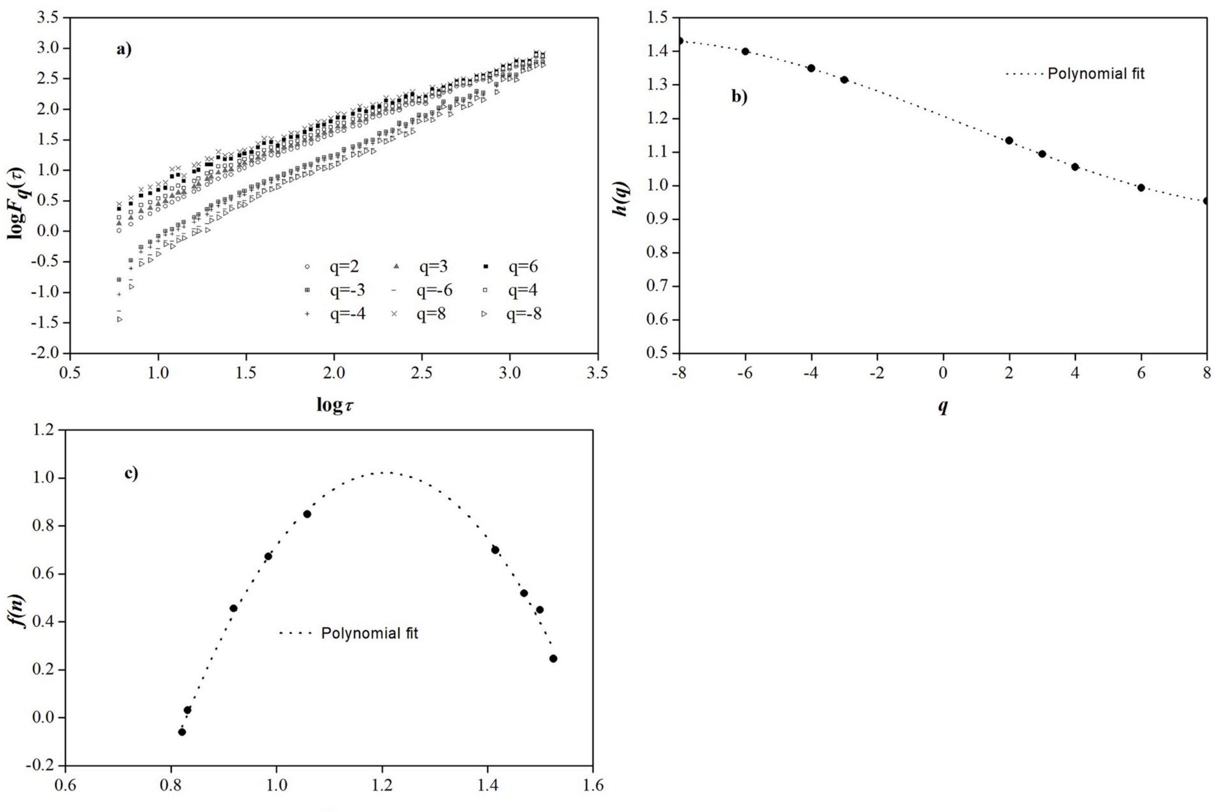

Fig. 6. a) The log-log plots of the MF-DFA2 fluctuation factor $F_q(\tau)$ versus the time scale s for specific moments q for the CR_{net} time series (at JNM64NM). b) Generalized Hurst exponent $h(q)$ versus q for the examined time series. The empirical curve (dots) is fitted by the polynomial of the third order ($y = 10^{-4}x^3 - 0.0002x^2 - 0.039x + 1.21$, with $R^2 = 0.999$) (solid line). c) The singularity spectrum $f(n)$ versus the singularity strength n for the examined time series. The empirical curve (dots) is fitted by the polynomial of the third order ($y = -0.033x^3 – 7.08x^2 + 17.2x – 9.37$, with $R^2 = 0.99$) (solid line, lower left).

36°S, 38°N).

Our first step was to apply the non-parametric Spearman's rank test to determine the correlation coefficient r_s between CR values (at A.Ne.Mo.S) and CRM values as well as between CR values (at A.Ne.Mo.S) and COTLM values. For the first case, the extracted coefficient was $r_s = -0.016$ suggesting thus that the hypothesis H_o: $r_s = 0$ vs H_1: $r_s \neq 0$ might be accepted at 95% confidence level (its significance was tested using the *t*-test). Similarly, for the second case, the derived coefficient was $r_s = -0.03$ indicating a very week anti-correlation at 95% confidence level, while the hypothesis H_o might be accepted at 99% confidence level.

Our next step was to apply the above mentioned scaling analysis on the time series of both cloud physical parameters CRM and COTLM. Table 2 shows the extracted DFA2 exponents ($\alpha = 0.56 \pm 0.01$ for CRM and $\alpha = 0.57 \pm 0.01$ for COTLM) which denote weak persistent memory (but not of 1/f – type). Moreover, the two criteria proposed by Maraun

Table 1
Scaling features of CR_{net} time series at JNM64NMs and at OULU.

	DFA2 exponent	Constancy of "local slopes"	Power spectral density	MF-DFA2 results
CR_{net} (JIGYNM)	$y = 1.09x$ - 1.1 $R^2 = 0.99$	sufficient constancy after $\log\tau = 1.8$	$y = 5.6\cdot10^{-6}x^{-1.67}$ with $R^2 = 0.58$ $y = 1.33\cdot10^{-3}e^{-10.6x}$ with $R^2 = 0.51$	• Scaling behavior of $F_q(\tau)$ for all the selected positive (negative) moments q is almost the same for $\tau > 100$, but not for smaller time scales $\tau < 100$, where the slope of $F_q(\tau)$ increases for less positive (more negative) moments q. • $h(q)$ is not independent of q, while the $h(q)$ values which are higher than 0.5 indicate long-term persistence. • The slope of $h(q)$ for positive moments seems to be similar to that one of negative moments (the polynomial fit of the empirical curve is $y = 4\cdot10^{-5}x^3$ - $0.0005x^2$ - $0.028x$ + 1.12, with $R^2 = 0.996$). • The maximum value of *f(n)* corresponds to $q = 0$ and *f(n)* fluctuates similarly on both sides of its maximum value (the polynomial fit of the empirical curve is $y = 0.78x^3$ - $11.58x^2 + 22.7x - 11$, with $R^2 = 0.994$).
CR_{net} (OULU)	$y = 1.11x$ - 1.3 $R^2 = 0.996$	sufficient constancy after $\log\tau = 1.8$	$y = 3.08\cdot10^{-6}x^{-1.63}$ with $R^2 = 0.58$ $y = 6.46\cdot10^{-4}e^{-10.4x}$ with $R^2 = 0.52$	• Scaling behavior of $F_q(\tau)$ for all the selected positive (negative) moments q is almost the same for $\tau > 100$, but not for smaller time scales $\tau < 100$, where the slope of $F_q(\tau)$ increases for less positive (more negative) moments q. • $h(q)$ is not independent of q, while the $h(q)$ values which are higher than 0.5 indicate long-term persistence. • The slope of $h(q)$ for positive moments seems to be similar to that one of negative moments (the polynomial fit of the empirical curve is $y = 9\cdot10^{-5}x^3$ - $0.0006x^2$ - $0.034x$ + 1.16, with $R^2 = 0.997$). • The maximum value of *f(n)* corresponds to $q = 0$ and *f(n)* fluctuates similarly on both sides of its maximum value (the polynomial fit of the empirical curve is $y = 2.38x^3$ - $15.4x^2 + 25.7x - 11.9$, with $R^2 = 0.99$).

et al. (2004) revealed constancy of local slopes for both time series and marginal rejection of the exponential fit only for the COTLM power spectral density (see Table 2).

As far as the spectrum of singularities for the COTLM and CRM time series, we used again the MF-DFA2 technique which gave a little different results from those ones of CR_{net} time series at A.Ne.Mo.S (see Table 2). In more detail, scaling behavior of $F_q(\tau)$ for all the selected positive (negative) moments q is almost the same for $\tau > 100$, but not for smaller time scales $\tau < 100$, where the slope of $F_q(\tau)$ increases for less positive (more negative) moments q (indicating multifractality for smaller time scales). Also, $h(q)$ values are higher than 0.5 suggesting long-term persistence. However, the slope of $h(q)$ for positive moments seems to be a little different from that one of negative moments, as well as the maximum value of *f(n)* corresponds to $q = 8$ and *f(n)* doesn't fluctuate similarly on the two sides of its maximum value. This fact reveals different features of multifractality for positive and negative q-values. These findings seem to agree with Laken et al. (2009) who, rejecting Svensmark et al. (2009), claim that the observed changes in COTLM are not causally related with cosmic ray variations. In addition, these findings seem to agree also with Kancirova and Kudela (2014) who concluded that there is no strong binding between cloud coverage and cosmic ray intensity during an interval of three solar activity cycles. In this point it is important to note that when daily means are averaged, the correlation increases systematically, but its positive value is significantly different from zero just when the averaging is done over about a year. However, at such time scales the similar value of correlation is found also with the sunspot number. Thus the other influences as e.g. solar irradiance can be connected with that dependence. For the cosmic ray decreases no clear connection to the decrease in cloud cover on the scale of several days has been found. The most intense ground level event ever observed at Lomnický štít (GLE 42) NM station with about 16% increase in daily means of the cosmic ray intensity, was accompanied by the profile of cloud cover indicating its higher level during the day of the GLE event and higher average level after than before the event.

4. Conclusions

We investigated the intrinsic self-similarity and the spectrum of singularities of cosmic ray time series at four NM stations: Athens NM64, Jungfraujoch IGY, Jungfraujoch NM64 and Oulu NM64, for the period 2000–2017. The techniques employed were DFA2 and MF-DFA2. The main conclusion obtained is that cosmic rays temporal evolution exhibits positive long-range correlations of 1/f type and multifractal behavior which were detected at all monitoring stations used in this research. As these stations are situated at different latitudes of North Hemisphere it could be claimed that this behavior is characteristic of CR at North Hemisphere. It should be noted at this point that the 1/f behavior may be encountered everywhere from atomic physics to astrophysics but its physical origin remains largely mysterious (Vernotte and Lantz, 2015).

In particular, the application of MF-DFA2 technique showed a great degree of multifractality only for smaller time scales ($\tau \leq 100$), a fact that is expected as the large windows cross several local periods with both small and large fluctuations (i.e. negative and positive q, respectively) and will therefore average out their differences in magnitude. However, common features of multifractality were revealed for both positive and negative q-values.

In the following, we tried to compare CR_{net} time series at A.Ne.Mo.S with the time series of two cloud physical parameters, however without detecting any statistically significant correlation. On the other hand, studying their scaling properties, a week persistent memory (but not of 1/f – type) was derived for both COTLM and CRM time series and MF-DFA2 revealed different features of multifractality for positive and negative q-values for each cloud parameter. In order to clarify whether the above-mentioned long-range correlations stem from the real values of the parameters used or from their temporal evolution we randomly shuffled the data and the derived DFA results did not change. It proves that the long-range correlations come from the real data and not from their temporal evolution.

It is also important to note that although investigations related to possible GCRs and clouds association have improved the understanding of cloud microphysical phenomena, the net effects of GCRs on clouds remain insufficiently understood (Pierce, 2017; Frigo et al., 2018).

The results obtained may enhance the fidelity of the sophisticated models not only for the dynamics of the cosmic rays, but also to the study of geophysical and solar parameters that are closely associated with cosmic rays (Kondratyev et al., 1994; Varotsos, 1994, 1998; Efstathiou and Varotsos, 2013). For example the above-mentioned results might give more information about the claimed difference in the solar activity evolution during odd and even solar activity cycles (Varotsos and Cracknell, 2004).

In addition, the obtained results confirm that NM stations' specifications like their geographical location and effective vertical cutoff rigidity, do not affect intrinsic properties of the recorded data like self-

Table 2
Scaling features of CRM and COTLM time series.

	DFA2 exponent	Constancy of "local slopes"	Power spectral density	MF-DFA2 results
CRM	$y = 0.56x - 1.78$ $R^2 = 0.99$	sufficient constancy after $\log\tau = 1.5$	$y = 3.2{\cdot}10^{-7}{\cdot}x^{-0.24}$ with $R^2 = 0.28$ $y = 7.3{\cdot}10^{-7}{\cdot}e^{-1.68x}$ *with* $R^2 = 0.29$	• Scaling behavior of $F_q(\tau)$ for all the selected positive moments q is almost the same for $\tau > 100$, but not for smaller time scales $\tau < 100$, where the slope of $F_q(\tau)$ increases. Similar results were extracted for the selected negative moments q. • $h(q)$ values are higher than 0.5 suggesting long-term persistence. • The slope of $h(q)$ for positive moments seems to be a little different from that one of negative moments (the polynomial fit of the empirical curve is $y = 3{\cdot}10^{-4}x^3 + 9{\cdot}10^{-4}x^2 - 0.056x + 0.69$, with $R^2 = 0.997$). • The maximum value of *f(n)* corresponds to $q = 8$ *revealing different features of multifractality for positive and negative q-values* (the polynomial fit of the empirical curve is $y = 15.8x^3 - 49.6x^2 + 45.66x - 10.9$, with $R^2 = 0.89$).
COTLM	$y = 0.57x + 0.37$ $R^2 = 0.99$	sufficient constancy after $\log\tau = 1.5$	$y = 6.1{\cdot}10^{-3}{\cdot}x^{-0.28}$ with $R^2 = 0.41$ $y = 1.5{\cdot}10^{-2}{\cdot}e^{-1.69x}$ *with* $R^2 = 0.32$	• Scaling behavior of $F_q(\tau)$ for all the selected positive moments q is almost the same for $\tau > 100$, but not for smaller time scales $\tau < 100$, where the slope of $F_q(\tau)$ increases. Similar results were extracted for the selected negative moments q. • $h(q)$ values are higher than 0.5 suggesting long-term persistence. • The slope of $h(q)$ for positive moments seems to be a little different from that one of negative moments (the polynomial fit of the empirical curve is $y = 3{\cdot}10^{-4}x^3 + 9{\cdot}10^{-4}x^2 - 0.056x + 0.69$, with $R^2 = 0.997$). • The maximum value of *f(n)* corresponds to $q = 8$ *revealing different features of multifractality for positive and negative q-values* (the polynomial fit of the empirical curve is $y = 6.02x^3 - 24.8x^2 + 24.4x - 5.99$, with $R^2 = 0.97$).

similarity and spectrum of singularities. Based on this conclusion, we can argue that for such a kind of statistical study of the CR time series the use of a data set originating from a particular station can lead to conclusions expressing the overall intrinsic characteristics of CR at North Hemisphere.

Acknowledgements

We acknowledge the NMDB database (www.nmdb.eu), founded under the European Union's FP7 program (grant number 213007) for providing cosmic ray data. Athens neutron monitor data were kindly provided by the Physics Faculty of the National and Kapodistrian University of Athens. Jung IGY and NM64 neutron monitor data were kindly provided by the Sphinx Observatory Jungfraujoch, while Oulu NM64 cosmic ray data were kindly provided by the University of Oulu. This research did not receive any specific grant from funding agencies in the public, commercial, or not-for-profit sectors.

Appendix A. Supplementary data

Supplementary data to this article can be found online at https://doi.org/10.1016/j.jastp.2019.04.012.

References

Anderson, T.W., Darling, D.A., 1954. A test of goodness of fit. J. Am. Stat. Assoc. 49, 765–769.

Baumgaertner, A.J.G., Seppälä, A., Jöckel, P., Clilverd, M.A., 2011. Geomagnetic activity related NO x enhancements and polar surface air temperature variability in a chemistry climate model: modulation of the NAM index. Atmos. Chem. Phys. 11 (9), 4521–4531.

Carslaw, K.S., Harrison, R.G., Kirkby, J., 2002. Cosmic rays, clouds, and climate. Science 298 (5599), 1732–1737.

Chattopadhyay, G., Midya, S.K., Chattopadhyay, S., 2019. MLP based predictive model for surface ozone concentration over an urban area in the Gangetic West Bengal during pre-monsoon season. J. Atmos. Sol. Terr. Phys. 184, 57–62.

Cracknell, A.P., Krapivin, V.F., Varotsos, C., 2009. Global Climatology and Ecodynamics: Anthropogenic Changes to Planet Earth. Springer-Praxis books in environmental sciences. Springer ; Published in association with Praxis Pub, Berlin ; New York , Chichester, UK.

Cracknell, A.P., Varotsos, C.A., 2007. Editorial and cover: fifty years after the first artificial satellite: from Sputnik 1 to ENVISAT. Int. J. Remote Sens. 28, 2071–2072. https://doi.org/10.1080/01431160701347147.

Efstathiou, M.N., Tzanis, C., Cracknell, A.P., Varotsos, C.A., 2011. New features of land and sea surface temperature anomalies. Int. J. Remote Sens. 32, 3231–3238. https://doi.org/10.1080/01431161.2010.541504.

Efstathiou, M.N., Varotsos, C.A., 2013. On the 11 year solar cycle signature in global total ozone dynamics: eleven-year solar cycle signature to global total ozone dynamics. Meteorol. Appl. 20, 72–79. https://doi.org/10.1002/met.1287.

Efstathiou, M.N., Varotsos, C.A., 2010. On the altitude dependence of the temperature scaling behaviour at the global troposphere. Int. J. Remote Sens. 31, 343–349. https://doi.org/10.1080/01431160902882702.

Frigo, E., Antonelli, F., da Silva, D.S., Lima, P., Pacca, I.I., Bageston, J.V., 2018. Effects of solar activity and galactic cosmic ray cycles on the modulation of the annual average temperature at two sites in southern Brazil. Ann. Geophys. 36 (2), 555–564.

Ihlen, E.A.F., 2012. Introduction to multifractal detrended fluctuation analysis in Matlab. Front. Physiol. 3. https://doi.org/10.3389/fphys.2012.00141.

Jackman, C.H., Marsh, D.R., Kinnison, D.E., Mertens, C.J., Fleming, E.L., 2016. Atmospheric changes caused by galactic cosmic rays over the period 1960–2010. Atmos. Chem. Phys. 16, 5853–5866. https://doi.org/10.5194/acp-16-5853-2016.

Kancirova, M., Kudela, K., 2014. Cloud cover and cosmic ray variations at Lomnický štít high altitude observing site. Atmos. Res. 149, 166–173. https://doi.org/10.1016/j.atmosres.2014.06.004.

Kantelhardt, J.W., Zschiegner, S.A., Koscielny-Bunde, E., Havlin, S., Bunde, A., Stanley, H.E., 2002. Multifractal detrended fluctuation analysis of nonstationary time series. Phys. A 316, 87–114. https://doi.org/10.1016/S0378-4371(02)01383-3.

Kondratyev, K.Y., Varotsos, C.A., Cracknell, A.P., 1994. Total ozone amount trend at St Petersburg as deduced from Nimbus-7 TOMS observations. Int. J. Remote Sens. 15, 2669–2677. https://doi.org/10.1080/01431169408954274.

Krapivin, V.F., Varotsos, C.A., Soldatov, V.Y., 2015. New Ecoinformatics Tools in Environmental Science. Springer International Publishing, Cham. https://doi.org/10.1007/978-3-319-13978-4.

Kudela, K., Flükiger, E.O., Torsti, J., Debrunner, H., 1996. On the character of cosmic ray variations at f>2·10-5 Hz. Nonlinear Process Geophys. 3, 135–141.

Kudela, K., Storini, M., Antalova, A., Rybák, J., 2001. On the wavelet approach to cosmic ray variability. In: Proceedings of ICRC.

Kudela, K., Venkatesan, D., 1995. Fractal structure of cosmic ray intensity variations. Nucl. Phys. B-Proc. Suppl. 39, 127–135.

Kudela, K., Venkatesan, D., 1993. On scaling temporal variations in cosmic ray intensity. Geophys. Res. Lett. 20, 2793–2796. https://doi.org/10.1029/93GL00090.

Laken, B., Wolfendale, A., Kniveton, D., 2009. Cosmic ray decreases and changes in the liquid water cloud fraction over the oceans. Geophys. Res. Lett. 36. https://doi.org/10.1029/2009GL040961.

Maraun, D., Rust, H.W., Timmer, J., 2004. Tempting long-memory-on the interpretation of DFA results. Nonlinear Process Geophys. 11, 495–503.

Mavromichalaki, H., 2010. Worldwide integration of neutron monitors. Eos Trans. Am. Geophys. Union 91, 305–306.

Mavromichalaki, H., Gerontidou, M., Mariatos, G., Papailiou, M., Papaioannou, A., Plainaki, C., Sarlanis, C., Souvatzoglou, G., 2009. Athens neutron monitor data processing center – ANMODAP center. Adv. Space Res. 44, 1237–1246. https://doi.org/10.1016/j.asr.2009.02.018.

Mavromichalaki, H., Preka-Papadema, P., Petropoulos, B., Tsagouri, I., Georgakopoulos, S., Polygiannakis, J., 2003. Low-and high-frequency spectral behavior of cosmic-ray intensity for the period 1953–1996. In: Annales Geophysicae. Copernicus GmbH, pp. 1681–1689.

Mavromichalaki, H., Sarlanis, C., Souvatzoglou, G., Tatsis, S., Belov, A., Eroshenko, E., Yanke, V., Pchelkin, A., 2001. Athens Neutron Monitor and its aspects in the cosmic-ray variations studies. Proc. 27th ICRC 10, 4099–4102.

Mavromichalaki, H., Gerontidou, M., Paschalis, P., Paouris, E., Tezari, A., Grosby, N., Dierckxsens, M., 2018. Real-time detection of the ground level enhancement on 10 September 2017 by ANeMoS: system report. Space Weather 16. https://doi.org/10.1029/2018SW001992.

McCracken, K.G., McDonald, F.B., Beer, J., Raisbeck, G., Yiou, F., 2004. A phenomenological study of the long-term cosmic ray modulation, 850–1958 AD. J. Geophys. Res. 109. https://doi.org/10.1029/2004JA010685.

Paschalis, P., Mavromichalaki, H., Dorman, L.I., Plainaki, C., Tsirigkas, D., 2014. Geant4 software application for the simulation of cosmic ray showers in the Earth's atmosphere. N. Astron. 33, 26–37. https://doi.org/10.1016/j.newast.2014.04.009.

Peng, C.-K., Buldyrev, S.V., Havlin, S., Simons, M., Stanley, H.E., Goldberger, A.L., 1994. Mosaic organization of DNA nucleotides. Phys. Rev. E 49, 1685.

Pierce, J.R., 2017. Cosmic rays, aerosols, clouds, and climate: recent findings from the CLOUD experiment. J. Geophys. Res.-Atmos. 122, 8051–8055.

Pierce, J.R., Adams, P.J., 2007. Efficiency of cloud condensation nuclei formation from ultrafine particles. Atmos. Chem. Phys. 7, 1367–1379.

Sarlis, N.V., Skordas, E.S., Varotsos, P.A., Nagao, T., Kamogawa, M., Tanaka, H., Uyeda, S., 2013. Minimum of the order parameter fluctuations of seismicity before major earthquakes in Japan. Proc. Natl. Acad. Sci. 110 (34), 13734–13738.

Schrijver, C.J., Derosa, M.L., 2002. What is missing from our understanding of long-term solar and heliospheric activity? Astrophys. J. 577, 1006.

Simpson, J.A., 2000. The cosmic ray nucleonic component: the invention and scientific uses of the neutron monitor. In: Cosmic Rays and Earth. Springer, pp. 11–32.

Solanki, S.K., Schüssler, M., Fligge, M., 2002. Secular variation of the Sun's magnetic flux. Astron. Astrophys. 383, 706–712. https://doi.org/10.1051/0004-6361:20011790.

Souvatzoglou, G., Papaioannou, A., Mavromichalaki, H., Dimitroulakos, J., Sarlanis, C., 2014. Optimizing the real-time ground level enhancement alert system based on neutron monitor measurements: introducing *GLE Alert Plus*. Space Weather 12, 633–649.

Stephens, M.A., 1974. EDF statistics for goodness of fit and some comparisons. J. Am. Stat. Assoc. 69, 730–737. https://doi.org/10.1080/01621459.1974.10480196.

Svensmark, H., Bondo, T., Svensmark, J., 2009. Cosmic ray decreases affect atmospheric aerosols and clouds. Geophys. Res. Lett. 36, L15101. https://doi.org/10.1029/2009GL038429.

Svensmark, J., Enghoff, M.B., Shaviv, N.J., Svensmark, H., 2016. The response of clouds and aerosols to cosmic ray decreases. J. Geophys. Res. Space Phys. 121, 8152–8181. https://doi.org/10.1002/2016JA022689.

Tidblad, J., Kucera, V., Ferm, M., Kreislova, K., Brüggerhoff, S., Doytchinov, S., Screpanti, A., Grøntoft, T., Yates, T., de la Fuente, D., Roots, O., Lombardo, T., Simon, S., Faller, M., Kwiatkowski, L., Kobus, J., Varotsos, C., Tzanis, C., Krage, L., Schreiner, M., Melcher, M., Grancharov, I., Karmanova, N., 2012. Effects of air pollution on materials and cultural heritage: ICP materials celebrates 25 Years of research. Int. J. Corros. 1–16, 2012. https://doi.org/10.1155/2012/496321.

Timmer, J., König, M., 1995. On generating power law noise. Astron. Astrophys. 300, 707–710.

Varotsos, C., 2005. Power-law correlations in column ozone over Antarctica. Int. J. Remote Sens. 26, 3333–3342. https://doi.org/10.1080/01431160500076111.

Varotsos, C., 2002. The southern hemisphere ozone hole split in 2002. Environ. Sci. Pollut. Res. 9, 375–376. https://doi.org/10.1007/BF02987584.

Varotsos, C., 1994. Solar ultraviolet radiation and total ozone, as derived from satellite and ground-based instrumentation. Geophys. Search Lett. 21, 1787–1790. https://doi.org/10.1029/93GL02090.

Varotsos, C., Assimakopoulos, M.-N., Efstathiou, M., 2007. Long-term memory effect in the atmospheric CO 2 concentration at Mauna Loa. Atmos. Chem. Phys. 7, 629–634. https://doi.org/10.5194/acp-7-629-2007.

Varotsos, C., Cartalis, C., 1991. Re-evaluation of surface ozone over Athens, Greece, for the period 1901–1940. Atmos. Res. 26, 303–310. https://doi.org/10.1016/0169-8095(91)90024-Q.

Varotsos, C., Efstathiou, M., Tzanis, C., 2009. Scaling behaviour of the global tropopause. Atmos. Chem. Phys. 9, 677–683. https://doi.org/10.5194/acp-9-677-2009.

Varotsos, C., Ondov, J., Efstathiou, M., 2005. Scaling properties of air pollution in Athens, Greece and Baltimore, Maryland. Atmos. Environ. 39, 4041–4047. https://doi.org/10.1016/j.atmosenv.2005.03.024.

Varotsos, C., Tzanis, C., Cracknell, A., 2009. The enhanced deterioration of the cultural heritage monuments due to air pollution. Environ. Sci. Pollut. Res. 16, 590–592. https://doi.org/10.1007/s11356-009-0114-8.

Varotsos, C.A., 1998. Total ozone and solar ultraviolet radiation, as derived from satellite and ground-based instrumentation at Dundee, Scotland. Int. J. Remote Sens. 19, 3301–3305. https://doi.org/10.1080/014311698213984.

Varotsos, C.A., Cracknell, A.P., 2004. New features observed in the 11-year solar cycle. Int. J. Remote Sens. 25, 2141–2157. https://doi.org/10.1080/014311603100011 5067.

Varotsos, C.A., Efstathiou, M.N., Cracknell, A.P., 2013. On the scaling effect in global surface air temperature anomalies. Atmos. Chem. Phys. 13, 5243–5253. https://doi.org/10.5194/acp-13-5243-2013.

Varotsos, C.A., Efstathiou, M.N., Cracknell, A.P., 2013. Plausible reasons for the inconsistencies between the modeled and observed temperatures in the tropical troposphere. Geophys. Res. Lett. 40, 4906–4910. https://doi.org/10.1002/grl.50646.

Varotsos, C.A., Ondov, J.M., Cracknell, A.P., Efstathiou, M.N., Assimakopoulos, M.-N., 2006. Long-range persistence in global Aerosol Index dynamics. Int. J. Remote Sens. 27, 3593–3603. https://doi.org/10.1080/01431160600617236.

Varotsos, P.A., Sarlis, N.V., Skordas, E.S., 2003. Long-range correlations in the electric signals that precede rupture: further investigations. Phys. Rev. E 67. https://doi.org/10.1103/PhysRevE.67.021109.

Vernotte, F., Lantz, E., 2015. Metrology and 1/f noise: linear regressions and confidence intervals in flicker noise context. Metrologia 52 (2), 222–237.

Weber, R.O., Talkner, P., 2001. Spectra and correlations of climate data from days to decades. J. Geophys. Res. 106, 20131–20144. https://doi.org/10.1029/2001JD000548.

Xanthakis, J., Mavromichalaki, H., Petropoulos, B., 1989. Time-evolution of cosmic-ray intensity modulation. Sol. Phys. 122, 345–363. https://doi.org/10.1007/BF00913001.